FULL PAPER

ADVANCED FUNCTIONAL MATERIALS

DOI: 10.1002/adfm.200500845

High-Quality Photonic Crystals Infiltrated with Quantum Dots**

By *Chantal Paquet*, *Fumiyo Yoshino*, *Larissa Levina*, *Ilya Gourevich*, *Edward H. Sargent*, and *Eugenia Kumacheva**

We report a method for producing colloidal crystals heavily loaded with PbS quantum dots (QDs). The approach employed uses capillary forces to load the QDs in the interstitial voids of the colloid crystals and yields highly ordered structures with a high loading of QDs. The infiltration process is qualitatively monitored using confocal fluorescence microscopy and scanning electron microscopy. The optical properties of the resulting composite structure are examined using optical spectroscopy. The shift in the stopband resulting from the infiltration of the colloid crystal shows that the PbS QDs occupy nearly 100 % of the volume of the interstitial space.

1. Introduction

Photonic colloidal crystals (PCCs) doped with semiconductor quantum dots (QDs) provide a possibility to couple optical resonances of photonic crystals and electronic resonances of QDs.[1–12] When the photonic crystal is loaded with QDs that possess nonlinear optical properties, the nanoparticles impart a photorefractivity to the PCC and as a result, allow light-induced control of transmission through the crystal. This feature offers a promising route to all-optical limiting and switching.[13–15]

Self-assembly of submicrometer-sized colloidal particles offers benefits to fabricating PCCs, such as simplicity, low cost, and growth of large-area crystals. Incorporation of QDs in the interstitial voids of such PCCs poses, however, two challenges in preserving the high crystalline quality of the PCC and achieving high loading of QDs. Two major strategies have been used to incorporate QDs in photonic crystals formed by the colloid self-assembly. In the first approach, microspheres carrying QDs either on the surface or in the interior were self-assembled into a PCC.[16–19] This approach yielded high-quality colloid crystals, yet, with a relatively low loading of QDs. In the second method, QDs were infiltrated into the interstitial voids of preformed colloidal crystals.[20–22] Since these works reported on the modification of the luminescence properties of the PCC, the extent of QD infiltration in these PCCs was not well characterized. Herein, we report on a route for the fabrication of PCCs with a high crystal quality and a high loading of QDs. We detail the characterization of the QDs, describe the challenges of infiltrating QDs into the PCC, and report the transmission properties of the resulting PCCs.

2. Results and Discussion

We infiltrated the PCCs with PbS QDs whose size-dependent excitons and Kerr nonlinearity are located in the near-IR spectral range. The size of PbS QDs can be controlled during their synthesis. This feature allows the spectral location of the exciton and Kerr nonlinearity of the QDs to coincide with the telecommunication range.[23,24] We used the procedure of Hines and Scholes[25] to prepare PbS QDs with diameters from 2.5 to 6.0 nm and with a polydispersity below 10 %.

Previously, we found a maximum change in the nonlinear refractive index of 4×10^{-4} for 5.2 nm sized PbS QDs (exciton peak at 1330 nm), which occurred 80 nm away from the exciton peak.[23] In the present work, the design of the QD-infiltrated photonic crystal relies on spectrally matching the nonlinearity of the QDs with the stopband edge of the PCC loaded with QDs. Furthermore, a steep stopband edge of the colloidal crystal was required to achieve low loss, low threshold switching between the on- and off-states of the nonlinear PCC.[26] This feature was accomplished by choosing a sufficiently high refractive-index contrast between the QDs and the polymer spheres. The size and the refractive indices of the PbS QDs and

[*] Prof. E. Kumacheva, C. Paquet, I. Gourevich
Department of Chemistry
University of Toronto
80 St. George Street
Toronto, ON M5S 386 (Canada)
E-mail: ekumache@chem.utoronto.ca
Prof. E. Kumacheva
Department of Chemical Engineering and Applied Chemistry
University of Toronto
200 College Street, Toronto, ON M5S 3E5 (Canada)
Prof. E. Kumacheva
Institute of Biomaterials & Biomedical Engineering
University of Toronto
4 Taddle Creek Road, Toronto, ON M5S 3G9 (Canada)
Dr. F. Yoshino, Dr. L. Levina, Prof. E. H. Sargent
Department of Electrical and Computer Engeneering
University of Toronto
10 King's College Road
Toronto, ON M5S 3G4 (Canada)

[**] We thank Prof. D.W. McComb, Dr. E. Istrate, and Dr. M. Allard for useful discussions. CP acknowledges funding from NSERC Canada through the PGS D program. EK and EHS acknowledge NSERC Canada for support through the CRD program.

ADVANCED FUNCTIONAL MATERIALS

the colloid microspheres were varied to satisfy these two criteria.

The linear refractive index of spin-coated close-packed layers of PbS QDs stabilized with oleic acid was determined by using spectroscopic ellipsometry. We used empirical dispersion laws which provide a good estimate of the effective refractive index of the close-packed arrays of QDs.[27] Figure 1a shows the variation of the refractive index of the film as a function of the volume of PbS QDs, the latter determined by analysis of the transmission electron microscopy (TEM) images. The insets of Figure 1a show TEM images of PbS QDs with different diameters. When the volume of PbS QDs increased from 100 to 1350 nm^3 the refractive index of the array increased from 1.60 to 1.90. To interpret this trend, we note that we measured the effective refractive index of a medium comprising high-refractive-index PbS QDs stabilized by the low-refractive-index oleic acid ($n = 1.459$). Since the volume fraction of PbS in the layer of nanoparticles increased with an increasing diameter of the QDs, we believe that the size dependence of the refractive index of QDs was dominated by the change in their volume fraction in the film. Figure 1b shows the correlation between the spectral position of the exciton peak and the refractive index of the array of PbS QDs. This correlation arises because both the effective refractive index and the exciton peaks of PbS QDs depend on the size of the nanoparticles.[24]

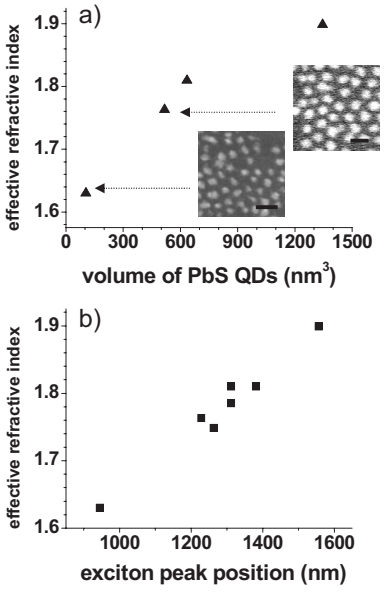

Figure 1. The effective refractive index of the close-packed film of PbS QDs as a function of a) the volume of individual PbS QDs and b) the spectral position of the exciton peak. The TEM images in a) show the characteristic morphology of the PbS QD diameters (scale bar 10 nm). The refractive index is quoted at 80 nm beyond the exciton peak where the effect of resonance, which produces anomalous dispersion, is negligible.

We produced colloidal crystals by the self-assembly of poly(methyl methacrylate) (PMMA) or polystyrene (PS) microspheres with diameters ranging from 400 to 600 nm.[28] The transmission spectra of the colloid crystals typically showed stopbands with attenuations of ca. 9 dB of light incident on the crystal. Figure 2a, curve i shows a representative transmission spectrum of the colloidal crystal prior to the infiltration of PbS QDs.

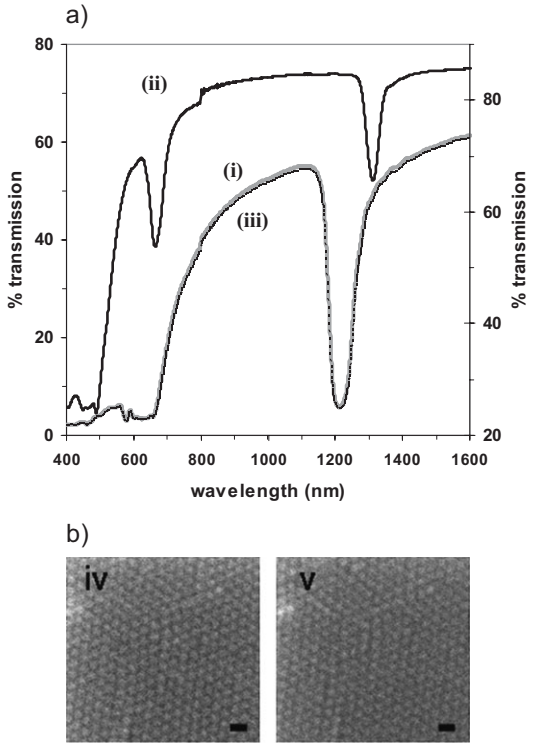

Figure 2. a) Transmission spectra of an 18 μm thick colloidal crystal produced from 575 nm sized PMMA microspheres: before infiltration with hexane (i), with infiltrated hexane (ii), and after hexane evaporation (iii). Spectra (i) and (iii) are nearly identical, indicating that infiltration of the interstitial space with hexane does not modify the crystal structure. b) Confocal fluorescence microscopy (CFM) images of a PCC infiltrated with hexane. Images represent crystal planes located 3.0 μm (iv), and 42 μm (v) below the top surface. The scale bars are 1 μm.

We found that incorporating QDs into the interstitial space of the colloid crystals was nontrivial when the goal was to achieve a high and uniform loading of QDs, without degradation of the crystalline lattice of the PCC. For instance, QDs deposited predominantly on the PCC surface when a preformed colloid crystal was immersed horizontally into a dispersion of QDs in hexane, and the solvent slowly evaporated. Similarly, QDs deposited preferentially on the surface of a PCC when the PCC was placed vertically into a dispersion of PbS QDs and infiltrated by the capillary rise of the dispersion. A successful method for the infiltration of PbS QDs into the PCC was as follows. A colloidal crystal grown on a glass slide was loosely covered with another glass slide and the sandwiched structure was placed vertically in a vial containing a dispersion of PbS QDs in hexane. Hexane was then allowed to evaporate at room temperature.[29] The capillary forces transported the QDs uniformly into the colloidal crystal, while the sandwich configuration prevented the nanoparticles from depositing on the surface of the PCC.

We selected hexane as the dispersant of the QDs for two reasons. First, hexane is a stable dispersant for PbS QDs stabilized with oleic acid. Second, hexane induces limited swelling of the polymer particles used as the building blocks of the colloid crystal. We verified that the PCC preserved its crystalline lattice and the QDs were restricted to the interstitial space of the PCC. Both features are demonstrated in Figure 2. First, to confirm that temporary infiltration of hexane did not distort the lattice of the colloid crystal built from PMMA microspheres, we acquired transmission spectra prior to infiltration, during infiltration, and after evaporating hexane from the colloid crystal (Fig. 2a, transmission spectra i–iii, respectively). Prior to infiltrating the colloid crystal with hexane, a stopband with an attenuation of 9.1 dB was centered at 1205 nm (Fig. 2a, spectrum i). Following infiltration of the crystal with hexane, the stopband broadened and red-shifted with respect to the initial position. Furthermore, the attenuation decreased from 9.1 to 1.0 dB (Fig. 2a, spectrum ii) and a second-order peak appeared at 655 nm. Prior to infiltration, this peak lay in the region of strong extinction caused mainly by coherent and incoherent scattering by the colloid crystal; following infiltration, the peak had shifted to a longer wavelength. The changes between spectrum i and ii were consistent with a decrease in the refractive-index contrast between colloidal particles and the interstitial space, as well as an increase in the effective refractive index of the colloidal crystal.[30] When hexane evaporated, the ultimate spectrum (Fig. 2a, spectrum iii) completely coincided with the original spectrum of the colloidal crystal; hence, we conclude that after infiltration of the colloid array with hexane the crystalline structure was preserved.

Next, we explored whether hexane infiltration occurred uniformly throughout the entire colloidal crystal. We immersed the colloid array in a hexane solution of a fluorescent dye 2-[methyl(7-nitro-2,1,3-benzodiazol-4-yl)-amino]ethanol (NBD-OH) and examined the structure of the dry colloidal crystal following hexane evaporation. Figure 2b shows typical confocal fluorescent microscopy (CFM) images acquired along the depth of the colloidal crystal. The distribution of the fluorescent signal through the PCC indicated uniform coating of the polymer microspheres with the dye and hence even infiltration of hexane in the interstitial space. Furthermore, the fluorescence images acquired in the *z*-direction of the PCC revealed that hexane penetrated downward into the crystal and was not localized at its surface. Similar results were obtained for colloidal crystals produced from PS microspheres.

We then proceeded to infiltrate the colloidal crystal with a dispersion of PbS QDs in hexane. Following evaporation of the solvent, the PCC acquired a dark-brown color (characteristic of the PbS QDs) while maintaining its characteristic iridescence. We examined the quality of infiltration of PbS QDs into the PCC with the aid of scanning electron microscopy (SEM). Comparison of typical SEM images of the top surface and cross sections of colloidal crystals before and after infiltration (Fig. 3a,c and 3b,d, respectively) shows efficient loading of PbS QDs in the interstitial space of the PCC. The image in Figure 3e captures pillars of QDs, which formed when the infiltrated PCC was cleaved into two parts and the PS microspheres were taken away leaving the infiltrated PbS behind. This image supports the results of CFM imaging: the PbS QDs were localized to the interstitial space of the PCC. Figure 3f shows a low-magnification image of a cross section of the infiltrated PCCs, which confirms uniform infiltration of PbS QDs along the depth of the crystal.

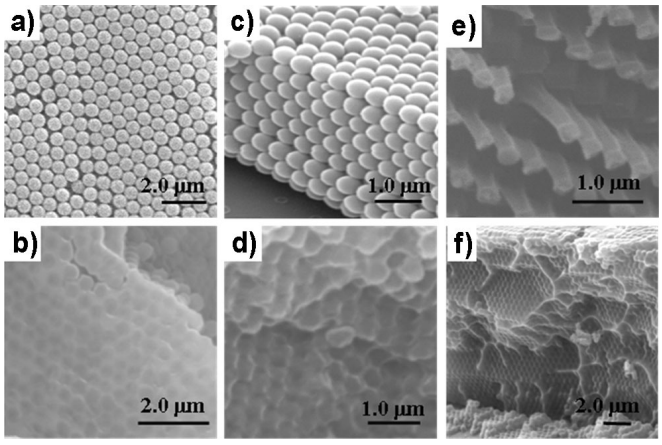

Figure 3. SEM images of the surface of a PCC before (a) and after (b) infiltration. Cross-sectional views of the crystal are shown before (c) and after (d) infiltration. Image (e) reveals pillars of PbS QDs which remained after an infiltrated PCC was cleaved. The infiltrated PCC in image (f) shows uniform infiltration of the large-area crystal.

We investigated the nature and origins of the optical properties of the PCC loaded with PbS QDs through a combination of measurements and simulation of the position of the stopband of PCC. At normal incidence, the spectral position of the stopband is a function of the refractive index of the microspheres (n_{sphere}) and the interstitial space of the PCC (n_{inf}). With an increasing degree of infiltration of the PCC with QDs, the value of n_{inf} increases from $n_{inf} = 1.0$ (air) to a value approaching the refractive index of PbS QDs of ca. 1.60–1.90 (this value is dependent on the size of QDs). The increase in n_{inf} leads to i) a red-shift of the stopband and ii) a decrease in the refractive-index contrast between the microspheres and the interstitial space, thereby decreasing the optical attenuation within the PCC.

By exploiting the fact that the stopband is a function of n_{inf}, we determined the extent of infiltration of PCC with QDs by determining the change in the spectral position of the stopband of the PCC prior to and after infiltration. First, a MULTEM simulation for a non-infiltrated PCC was carried out, using the refractive index of the polymer spheres and the interstitial space as inputs.[31] The stopband position obtained from the simulations was fit to the position of the experimentally measured stopband for the nonloaded colloidal crystal (at $n_{inf} = 1.00$). The value of n_{inf} in the simulations of the infiltrated crystal was then adjusted so that the transmission curve matched the measured transmission curve. The value of n_{inf}, found in

ADVANCED FUNCTIONAL MATERIALS

this manner, was then used to determine the degree of infiltration, ϕ_{QDs}, of the crystal according to Equation 1[32]

$$\frac{n_{inf}^2 - 1}{n_{inf}^2 + 2} = \varphi_{QDs} \frac{n_{QDs}^2 - 1}{n_{QDs}^2 + 2} \quad (1)$$

In Equation 1, the value of ϕ_{QDs} is a measure of the degree of infiltration: in the case of complete infiltration, $\phi_{QDs} = 1$ and $n_{inf} = n_{QDs}$, while for incomplete infiltration, $\phi_{QDs} < 1$ and $n_{inf} < n_{QDs}$. For a particular value of n_{inf} (found from the position of a stopband) we estimated the extent of infiltration of the PCC with QDs.

Figure 4a shows the transmission spectra of the PCC obtained from PS microspheres ($n_{sphere} = 1.59$)[33] before (solid line) and after (dotted line) infiltrating the colloid array with PbS QDs ($n_{QDs} = 1.63$). Following infiltration, a single exciton peak associated with the absorbance of the PbS QDs was measured at 945 nm and the dark-brown color of the PCC suggested that efficient infiltration had taken place. We stress that the stopband (originally centered at 1320 nm) disappeared due to a close match of the refractive index of the interstitial space filled with the QDs and the PS spheres. Based on Equation 1, we estimated that this PCC, perfect refractive index match occurred at 95 % infiltration with 2.9 nm sized PbS QDs.

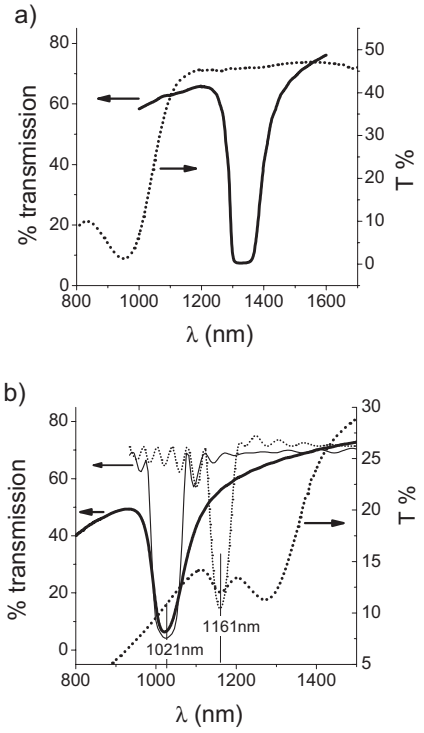

Figure 4. a) Transmission spectra of a colloidal crystal produced from 580 nm sized PS microbeads before (—) and after (···) infiltration with PbS QDs. The dip in transmission at 945 nm corresponds to the exciton energy of the QDs. b) Transmission of experimentally measured (—,···) and simulated (—, · · ·) spectra of PCC produced from 470 nm sized PMMA microspheres before (—, —) and after (···, · · ·) infiltration with PbS QDs. The peak at 1280 nm corresponds to the exciton peak of the PbS QDs.

By contrast, for the PCC formed from PMMA microbeads ($n_{sphere} = 1.49$),[33] a sufficient refractive-index contrast existed between the microspheres and the interstitial space of PCC infiltrated with PbS QDs to observe a stopband. The original colloid crystal had a stopband centered at 1021 nm, which shifted to 1161 nm after infiltration of the QDs (Fig. 4b). Based on the simulations, the 140 nm shift in the stopband corresponded to $n_{inf} = 1.70$. By using $n_{inf} = 1.70$ and $n_{QDs} = 1.76$, we found $\phi_{QDs} = 94\,\%$. Figure 4 shows the importance of the 'design'-based approach to the PCCs: the stopband can only be expected for a sufficiently high refractive-index contrast between the polymer spheres and the interstitial space of the PCC doped with QDs (the latter determined by the refractive index of the QDs, the degree of infiltration, and the refractive index of the polymer microspheres).

3. Conclusions

We designed and fabricated a high-quality photonic crystal heavily loaded with PbS QDs and examined its transmission properties. We used the shift in the stopband resulting from the infiltration of the PCC to determine the volume fraction of PbS QDs occupying the interstitial space. We demonstrated that the stopband position can be controlled by changing the refractive-index modulation in the PCC: by changing the refractive index of the microspheres, the effective refractive index of the QDs, and by varying the extent of infiltration of the PCC with QDs. To realize efficient all-optical limiting from these structure we are currently working on adjusting the alignment of the nonlinearity of the QDs to match the stopband edge of the infiltrated PCC.

4. Experimental

Materials: Methyl methacrylate (MMA), styrene, ethylene glycol dimethacrylate (EGDMA), 1-dodecanthiol, and ammonium persulfate, were purchased from Aldrich Canada and used without further purification. Hexanes (which were referred to as hexane in the text) were ACS grade, purchased from Uniscience. Ultrapure water (18.2 $M\Omega\,cm^{-1}$) was supplied using a Milli-Q water system. Lead oxide powder (10 μm, 99.9 %) and oleic acid (90 %), both used for the preparation of the lead precursor, and hexamethyldisilathiane, used as a sulfur precursor, were purchased from Aldrich Canada. The fluorescent dye NBD-OH was synthesized as described elsewhere [34]. PS colloids were purchased from Polysciences.

Synthesis and Characterization of Colloid Particles: PMMA particles were synthesized by surfactant-free emulsion polymerization. Colloid particles with a diameter smaller than 500 nm were synthesized under semibatch conditions; the microspheres larger than ca. 500 nm were obtained via multistage emulsion polymerization as described elsewhere [34]. The colloid particles were imaged using a Hitachi S-570 scanning electron microscope at an accelerating voltage of 15 kV and a working distance of 15 mm. The dispersions were dried onto an aluminium stub and coated with a thin layer of gold prior to SEM imaging. The average diameter and standard deviation in the microsphere sizes were obtained by analyzing the images using UTHSCSA Image Tool software.

Synthesis of QDs: The synthesis of PbS QDs was performed in a three-necked flask adjusted with a condenser and thermocouple. Lead oxide powder (0.45–0.90 g) was dissolved in 20–10 mL of oleic acid

under vigorous stirring at 150 °C. Hexamethyldisilathiane in octadecene (210–420 μL) was introduced into the reaction vessel in a single injection through a rubber septum. The rapid introduction of the sulfur source produced a dark-brown solution of PbS QDs with an exciton peak positioned between 1300 and 1600 nm. The final nanocrystals were isolated from the growth mixture by precipitation with methanol, and redispersed in toluene or hexane.

Colloidal-Crystal Growth: Microslides (3 in. × 1 in. × 1 mm) cut into quarters were cleaned in a piranha solution (1:3 H_2O_2/H_2SO_4) and rinsed thoroughly with Milli-Q water. Dried substrates were placed vertically into 20 mL scintillation vials containing 0.1–1.0 wt % colloid dispersions. The vials were covered with a beaker (250 mL) and placed in an oven at 65 °C. Evaporation of water from the dispersion generally took ca. 48 h.

Infiltration of PbS QDs in PCC: A colloidal photonic crystal was placed vertically into a scintillation vial. A glass slide, cut to the same dimensions as the substrate of the PCC, was placed vertically, gently touching the crystal in order to make a sandwich structure. The PbS QDs dispersed in hexane were added to the vial. The vial was loosely capped in order to allow solvent evaporation. Following hexane evaporation, PbS QDs deposited on the exterior surface of the glass substrates were removed with a solvent.

Characterization of Infiltrated PCC: The colloidal crystals loaded with fluorescent dyes were imaged with a Zeiss 510 inverted confocal fluorescence microscope (× 63 1.4NA immersion lens, a 488 nm line of an Argon laser as a source, detection in the range from 505 to 550 nm). The transmission spectra of the PCC crystal were determined using a Varian Cary 5000 UV/VIS/NIR spectrophotometer.

Characterizing PbS QDs: The PbS QDs were imaged using TEM by evaporating a dilute dispersion onto a TEM grid. The images were acquired on a Hitachi scanning transmission electron microscope (MD2000). The diameter and standard deviation of the QDs were obtained by analyzing their TEM images using UTHSCSA Image Tool software. The spectra of PbS QDs were acquired using a Varian Cary 5000 UV–vis–near-IR spectrometer. A Sopra GES-5 spectroscopic ellipsometer was used to obtain the optical constant of films of PbS QDs. Since the dimensions of the PbS QDs surrounded with the ligand films are well below the wavelength of light, we used a model which represented their films as a homogenous medium. The PbS and oleic acid ligands were collectively described by the Sellmeier law with superpositioned Lorentz harmonic oscillator peaks. Results obtained from ellipsometry were verified from Brewster-angle measurements.

Received: November 25, 2005
Final version: February 15, 2006
Published online: August 16, 2006

[1] Y. Lin, J. Zhang, E. H. Sargent, E. Kumacheva, *Appl. Phys. Lett.* **2002**, *81*, 3134.
[2] A. Blanco, C. López, R. Mayoral, H. Míguez, F. Meseguer, A. Mifsud, J. Herrero, *Appl. Phys. Lett.* **1998**, *73*, 1781.
[3] H. Míguez, A. Blanco, F. Meseguer, C. López, H. M. Yates, M. E. Pemble, V. Fornés, A. Mifsud, *Phys. Rev. B* **1999**, *59*, 1563.
[4] A. Blanco, H. Miguez, F. Meseguer, C. López, F. López-Tejeira, J. Sánchez-Dehesa, *Appl. Phys. Lett.* **2001**, *78*, 3181.
[5] S. G. Romanov, A. V. Fokin, R. M. De La Rue, *Appl. Phys. Lett.* **1999**, *74*, 1821.
[6] Y. A. Vlasov, K. Luterova, I. Pelant, B. Hönerlage, V. N. Astratov, *Appl. Phys. Lett.* **1997**, *71*, 1616.
[7] V. N. Astratov, A. M. Adawi, M. S. Skolnick, V. K. Tikhomirov, V. Lyubin, D. G. Lidzey, M. Ariu, A. L. Reynolds, *Appl. Phys. Lett.* **2001**, *78*, 4094.
[8] J. Zhou, Y. Zhou, S. Buddhudu, S. L. Ng, Y. L. Lam, C. H. Kam, *Appl. Phys. Lett.* **2000**, *76*, 3513.
[9] A. Rogach, A. Susha, F. Caruso, G. Sukhorukov, A. Kornowski, S. Kershaw, H. Möhwald, A. Eychmüller, H. Weller, T. Yamasaki, T. Tsutsui, *Appl. Phys.* **1998**, *72*, 1957.
[10] H. P. Schriemer, H. M. van Driel, A. F. Koenderink, W. L. Vos, *Phys. Rev. A* **2001**, *63*, 011 801.
[11] A. F. Koenderink, L. Bechger, H. P. Schriemer, A. Lagendijk, W. L. Vos, *Phys. Rev. Lett.* **2002**, *88*, 143 903.
[12] S. V. Gaponeńko, A. M. Kapitonov, V. N. Bogomolov, A. V. Prokofiev, A. Eychmüller, A. L. Rogach, *JETP Lett.* **1998**, *68*, 143.
[13] L. Brzozowski, E. H. Sargent, *IEEE J. Quantum Electron.* **2000**, *36*, 550.
[14] D. E. Pelinovsky, L. Brzozowski, E. H. Sargent, *Phys. Rev. E* **2000**, *62*, 4536.
[15] M. Soljacic, J. D. Joannopoulos, *Nat. Mater.* **2004**, *3*, 211.
[16] W. Wang, S. A. Asher, *J. Am. Chem. Soc.* **2001**, *123*, 12 528.
[17] J. Zhang, N. Coombs, E. Kumacheva, Y. Lin, E. H. Sargent, *Adv. Mater.* **2002**, *14*, 1756.
[18] A. L. Rogach, N. A. Kotov, D. S. Koktysh, A. S. Susha, F. Caruso, *Colloids Surf. A* **2002**, *202*, 135.
[19] Y. Chan, J. P. Zimmer, M. Stroh, J. S. Steckel, R. K. Jain, M. G. Bawendi, *Adv. Mater.* **2004**, *16*, 23.
[20] Y. A. Vlasov, N. Yao, D. J. Norris, *Adv. Mater.* **1999**, *11*, 165.
[21] A. L. Rogach, N. A. Kotov, D. S. Koktysh, J. W. Ostrander, G. A. Ragoisha, *Chem. Mater.* **2000**, *12*, 2721.
[22] Y. Yang, B. Yang, Z. Fu, H. Yan, W. Zhen, W. Dong, L. Xia, W. Liu, Z. Jian, F. Li, *J. Phys. Condens. Matter* **2004**, *16*, 7277.
[23] F. Yoshino, A. Major, L. Brzozowski, L. Levina, V. Sukhovatkin, E. H. Sargent, in *Proc. SPIE Quantum Dots, Nanoparticles, and Nanoclusters*, Vol. 5361 (Eds: D. L. Huffaker, P. Bhattacharya), SPIE, Bellingham, WA **2004**, pp. 142–149.
[24] F. W. Wise, *Acc. Chem. Res.* **2000**, *33*, 773.
[25] M. A. Hines, G. D. Scholes, *Adv. Mater.* **2003**, *15*, 1844.
[26] H. W. Tan, H. M. van Driel, S. L. Schweizer, R. B. Wehrspohn, U. Gösele, *Phys. Rev. B* **2004**, *70*, 205 110.
[27] C. Lü, C. Guan, Y. Liu, Y. Cheng, B. Yai, *Chem. Mater.* **2005**, *17*, 2448.
[28] P. Jiang, J. F. Bertone, K. S. Hwang, V. L. Colvin, *Chem. Mater.* **1999**, *11*, 2132.
[29] Personal communications with Professor D. W. McComb **2004**.
[30] Y. A. Vlasov, V. N. Astratov, O. Z. Karimov, A. A. Kaplyanskii, V. N. Bogomolov, A. V. Prokofiev, *Phys. Rev. B* **1997**, *55*, 13 357.
[31] N. Stefanou, V. Yannopapas, A. Modinos, *Comput. Phys. Commun.* **1998**, *113*, 49.
[32] A. G. Bruggeman, *Ann. Phys.* **1935**, *24*, 636.
[33] J. Brandrup, E. A. Grulke, E. H. Immergut, in *Polymer Handbook* (Eds: J. Brandrup, E. A. Grulke, E. H. Immergut), Wiley, New York **1999**, Ch. 6.
[34] O. Kalinina, E. Kumacheva, *Macromolecules* **1999**, *32*, 4122.